

# Optimizing hot carrier effects in Pt-decorated plasmonic heterostructures

Jorge U. Salmón-Gamboa,<sup>ID</sup>\* Mayela Romero-Gómez, Diane J. Roth, Matthew J. Barber,<sup>ID</sup> Pan Wang, Simon M. Fairclough,<sup>ID</sup> Mazhar E. Nasir, Alexey V. Krasavin, Wayne Dickson and Anatoly V. Zayats

Received 9th October 2018, Accepted 14th November 2018

DOI: 10.1039/c8fd00150b

Hot carrier generation by light in various semiconductors and metallic nanostructures is important for many photocatalytic and photochemical processes, including water and hydrogen splitting. Here, we report on investigations of hot electron generation and extraction from Pt decorated SiO<sub>2</sub>-Au nanoparticles using the degradation of methylene blue dye as a test-bed. Enhanced catalytic activity was found with an increase of Pt loading on the surface of the heterostructures. The small size of the Au nanoparticles (~12 nm) decorating the silica nanoparticles reduces hot electron collisions and related thermalization processes, since charge carriers have short paths to the surface where reactions take place and where Pt is situated. The heterostructures exhibit a broad plasmonic resonance in the visible wavelength range from 500 to 700 nm and hot carrier generation predominately takes place under resonant excitation. Electron-microscopy characterization and numerical modelling have allowed the optimization of Pt coverage for hot-electron transfer, consisting of a thin Pt shell covering the Au nanoparticle with Pt nanoparticles additionally placed on top. This geometry provides an increased number of active sites for methylene blue degradation and promotes separation of charge carriers generated by plasmonic excitations in Au. Such SiO<sub>2</sub>-Au-Pt nanoparticles are attractive for hot-electron production due to the tunability of their plasmonic resonance and enhanced catalytic activity.

## 1 Introduction

Heterogeneous photocatalysis by plasmonic nanoparticles is one of the most important processes using hot charge carriers.<sup>1-4</sup> Hydrogen generation by plasmon-assisted water splitting is amongst the most investigated processes.<sup>5-11</sup> The ability to dissociate diatomic hydrogen molecules at room temperature and atmospheric pressure by plasmonic nanoparticles<sup>12-14</sup> proved that well-designed plasmonic nanostructures are able to perform difficult chemical reactions in

*Department of Physics and London Centre for Nanotechnology, King's College London, Strand, London WC2R 2LS, UK. E-mail: jorge.salmon@kcl.ac.uk*

ambient conditions, which is of paramount interest for applications. Water purification from organic pollutants, using semiconductor-noble metal hybrids, has also been extensively studied, driven by the increasing demand for clean water sources needed for population growth and industrial development.<sup>15–17</sup>

While spherical Au nanoparticles have strong and distinct resonances in the short wavelength range, the spectral tunability and opportunity to engineer electron transfer at the interfaces are important requirements for catalytic applications. Spherical dielectric-Au core-shell nanoparticles, often referred to as Au nanoshells, are one of the simplest nano-sized plasmonic heterostructures. These can be easily synthesized in volume *via* chemical methods and offer remarkable optical properties,<sup>18</sup> which can be tuned by varying the size of the core dielectric or the shell thickness.<sup>19</sup> This gives the nanostructures the ability to absorb and scatter light throughout the visible and near-infrared spectral range. For this, Au nanoshells have been under a continuous study and their applications include biosensing, bioimaging and photothermal ablation of tissues and cells.<sup>20</sup> Since plasmonic resonances are sensitive to the immediate surroundings of the nanoparticle where the plasmonic field extends, modification of plasmonic resonances can be achieved by loading nanoparticles with even smaller nanoparticles of different materials.

In this paper, silica nanoparticles decorated with Au nanoparticles and Pt (from now on referred to as SiO<sub>2</sub>-Au-Pt heterostructures, schematic shown in Fig. 1a) were designed and optimized for the enhancement of hot-electron generation and extraction. Pt-Au heterostructures are often used to achieve an enhanced catalytic performance.<sup>9,10,21</sup> SiO<sub>2</sub>-Au-Pt nanoparticles are attractive for hot-electron production thanks to the tunability of their plasmonic resonance in the visible spectrum, and the use of SiO<sub>2</sub> cores has added the advantage of having an inert dielectric support for Au. In this case no Schottky barrier is formed, therefore more hot carriers are available for reduction processes, instead of migrating through a Schottky junction<sup>13</sup> if a semiconductor was used. The small size of the Au nanoparticles reduces hot electron collisions, due to short pathways to the surface, and related thermalisation processes. Furthermore, the addition of Pt on the surface of

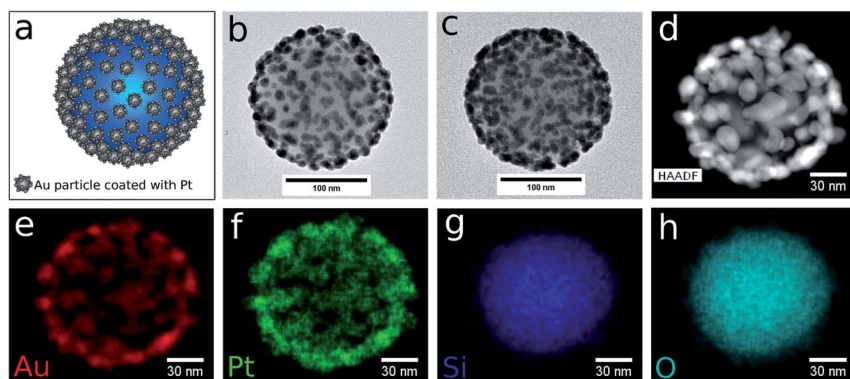


Fig. 1 (a) Schematic of the heterostructured nanoparticle. (b and c) TEM images of a single nanoparticle of SiO<sub>2</sub>-Au and SiO<sub>2</sub>-Au-Pt (sample Pt), respectively. (d) HAADF-STEM and (e–h) elemental mapping images of a SiO<sub>2</sub>-Au-Pt heterostructure (sample Pt+++).

Au delays electron–hole recombination *via* charge separation, which improves the functionality of plasmonic heterostructures as exhibited by photocatalytic activity assessments of the prepared catalysts for methylene blue photodegradation.

## 2 Experimental methods

### 2.1 Chemicals

Tetraethyl orthosilicate (TEOS, 98%), 200 proof ethanol, ammonium hydroxide solution (NH<sub>3</sub> in H<sub>2</sub>O, 28%), 3-aminopropyltriethoxysilane (APTES, 99%), tetrakis(hydroxymethyl)phosphonium chloride (THPC, 80% in water), Au(III) chloride trihydrate (HAuCl<sub>4</sub>·3H<sub>2</sub>O, 99.9%), hexachloroplatinic(IV) acid hexahydrate (H<sub>2</sub>PtCl<sub>6</sub>·6H<sub>2</sub>O, 99%), potassium carbonate (K<sub>2</sub>CO<sub>3</sub>, 99.995%), formaldehyde solution (CH<sub>2</sub>O, 37 wt% in H<sub>2</sub>O), sodium hydroxide (NaOH, 98%), sodium chloride (NaCl, 99%), L-ascorbic acid (C<sub>6</sub>H<sub>8</sub>O<sub>6</sub>, 99%), methylene blue solution (methylene blue, 1.5%), potassium iodide (KI, 99.5%), *p*-benzoquinone (BQ, 98%) and 2-propanol (2-Pr, 99.5%) were used as received from Sigma-Aldrich. Deionized (DI) water with a resistivity of 18.2 MΩ was used throughout the procedures, and all reactions were performed in air.

### 2.2 Synthesis of precursors and heterostructures

#### Precursor solutions

**Au seeds suspension.** The protocol followed for the synthesis of this solution is fully described and studied by Duff *et al.*<sup>22</sup> Briefly, 500 μL of 1 M NaOH was added into 45 mL of DI water while stirring at 900 rpm, followed by the addition of 1 mL of THPC (68 mM). After 5 minutes of constant stirring, 2 mL of 1 wt% HAuCl<sub>4</sub> solution was added. Immediately the solution turned to a dark brown colour and was left under stirring in the dark for a further 15 minutes. The mixture was then stored at 4 °C for a period of at least 2 weeks. The resultant solution is a colloidal suspension of 1–2 nm Au spherical seeds.

**Au plating solution (K–Au).** 12.42 mg of K<sub>2</sub>CO<sub>3</sub> was added into 50 mL of DI water, followed by the addition of 750 μL of 1 wt% HAuCl<sub>4</sub> solution. The mixture was then stirred at 900 rpm for 30 minutes and stored at 4 °C overnight before use.

**SiO<sub>2</sub> nanoparticles and APTES functionalization.** SiO<sub>2</sub> nanoparticles dispersed in ethanol were synthesized following the Stöber method.<sup>23</sup> First, 167.5 μL of TEOS was mixed with 1.33 mL of ethanol, while 38.1 μL of 28% ammonium hydroxide was mixed with 407.8 μL of DI water and 1.05 mL of ethanol. Subsequently the two solutions were mixed under constant stirring at 300 rpm for 210 min. This process resulted in monodisperse silica nanoparticles of approximately 155 nm in diameter. The mixture was centrifuged 3 times, at 9000 rpm for 15 min, and redispersed in 5 mL of ethanol. In order to obtain amine-terminated nanoparticles, organosilane molecules (APTES) were adsorbed on the surface of silica. For this purpose, 500 μL of the prepared solution of SiO<sub>2</sub> nanoparticles was mixed with 5 mL of ethanol and, under stirring for 10 min at 650 rpm, 10 μL of APTES was added. The mixture was then allowed to stir at 100 rpm overnight. Subsequently, the solution was heated to 90 °C whilst stirring for one hour, along with addition of ethanol during the synthesis which prevented total evaporation of the solvent. Finally, the nanoparticles were washed three times in ethanol by centrifugation at 8500 rpm for 15 min and redispersed in 2 mL of ethanol.

**SiO<sub>2</sub>-Au nanoparticles.** The procedure followed for the synthesis of SiO<sub>2</sub>-Au nanoshells was based on the framework outlined by Wang *et al.*<sup>24</sup> Herein the process of obtaining incomplete nanoshells (*i.e.* SiO<sub>2</sub>-cores decorated with discrete Au nanoparticles) is described as follows. The pH of a 3 mL solution of THPC-Au was adjusted to a pH of 3 by the addition of HCl to ensure interaction between the Au seeds and the amino-terminated silica cores. 60 μL of 1 M NaCl and 200 μL of APTES functionalized silica nanoparticles were added in the mixture, sonicated for 5 minutes and left undisturbed overnight. The mixture was centrifuged 3 times at 7500 rpm for 15 minutes and redispersed in 1 mL of DI water. The outcome of this procedure is a solution of colloidal silica cores decorated with 1–2 nm Au seeds. The resultant solution was refrigerated at 4 °C when not in use. In order to increase the size of the Au seeds attached on the surface of the cores, 3 mL of K-Au was added to 4 mL of the previously prepared seeded silica nanoparticles while stirring, followed by the addition of 50 μL of formaldehyde. The mixture was then left stirring for 15 more minutes and a change in colour, from pink to deep violet, was observed. The nanoparticles were immediately washed by centrifugation at 3000 rpm for 15 min and redispersed in 8 mL of DI water. As the result of this procedure, SiO<sub>2</sub>-Au nanoparticles with extinction around 560 nm were obtained. The colloidal solution was then stored at room temperature.

**SiO<sub>2</sub>-Au-Pt nanoparticles.** The coating of the nanoparticles with Pt requires ions provided by H<sub>2</sub>PtCl<sub>6</sub>, reduced by ascorbic acid, to produce the elemental form on the surface of the heterostructure. First, 200 μL of 0.1 M L-ascorbic acid and 6.5 μL of 10 mM H<sub>2</sub>PtCl<sub>6</sub> were mixed with 4 mL of SiO<sub>2</sub>-Au in a vial. The mixture was kept in a water bath at 70 °C for 3 hours and let to rest overnight. Finally, the mixture was centrifuged at 2700 rpm for 15 min and redispersed in 4 mL of DI water. Additional samples with different amounts of H<sub>2</sub>PtCl<sub>6</sub> were synthesized in order to study the effect of Pt loading on the efficiency of hot electron extraction. In addition to this sample designated as “sample Pt”, 13 μL (sample Pt+), 26 μL (sample Pt++) and 39 μL (sample Pt+++) of the Pt precursor were used to prepare the additional samples, under the same conditions described above. The final concentration of heterostructures of the samples was estimated to be around 0.15 nM.

### 2.3 Photocatalytic activity experiments

The hot carrier extraction of the synthesized heterostructures was investigated by photodegradation of methylene blue. During the degradation experiments, the absorbance maximum of methylene blue, located at 664 nm, was monitored over time, allowing the reaction kinetics to be studied. All photocatalysis studies were performed in a standard 1 cm × 1 cm fluorescence cell (Optical Glass 340–2500 nm) for 4 hours of irradiation at room temperature. A collimated super-continuum laser, of a beam diameter of 1 cm, was used as a light source to excite the plasmonic samples, and the optical absorption of methylene blue was recorded by a spectrometer. Optical filters were used to selectively control the excitation wavelength range. For all optical measurements, mixtures composed of 467 μL of 20 μM methylene blue, 333 μL of catalyst solution and 200 μL of DI water were prepared. The control experiment was carried out with a solution of 467 μL of 20 μM methylene blue mixed with 533 μL of DI water.

## 2.4 Materials characterization

Transmission electron microscopy (TEM) images were taken on JEOL F200 running at 200 kV. TEM electron dispersive X-ray spectroscopy (EDS) was performed using an Oxford Instruments EDS detector. The samples were prepared by drop casting the catalysts in methanol on to Agar Scientific carbon grids. Elemental maps were taken by scanning transmission electron microscopy (STEM) with EDS on a Titan G2 ChemiSTEM operating at 200 kV.

## 2.5 Numerical simulations

The extinction cross-section responses of individual  $\text{SiO}_2$ -Au and  $\text{SiO}_2$ -Au-Pt structures dispersed in water were obtained from far field calculations using the transient solver utilizing finite integration technique in time domain (CST Microwave studio). Dispersionless refractive index values were considered for  $\text{SiO}_2$  and water to be 1.4585 and 1.3325, respectively. The optical constant of Au was taken from experimentally measured tabulated values,<sup>25</sup> with a 5 nm mean free path correction taking into account the nanoscale size of the object, while the optical constant of Pt used was taken from experimental values reported by Werner *et al.*<sup>26</sup> The nanostructure was excited by a linearly polarized plane wavefront electromagnetic pulse with a broad spectrum, from 400 to 800 nm, and its response was investigated. To be able to retrieve the far field scattered light after the excitation, open space boundary conditions were set, on which minimal reflections are also ensured. Finally, from the obtained field distribution an extinction cross-section of the nanostructure was calculated.

# 3 Results and discussion

## 3.1 Characterization of heterostructures

Au nanostructures are of great interest due to the tunability of their optical extinction *via* the control of particle size, surrounding medium and morphology.<sup>27</sup> The type of heterostructure studied in this work features plasmon resonance in the visible spectrum and can be tuned by varying the size of the attached Au particles onto the silica matrix. Fig. 1b and c show the TEM images of single  $\text{SiO}_2$ -Au and  $\text{SiO}_2$ -Au-Pt heterostructures, respectively. The average size of the silica cores is around 155 nm, while the discrete decorating Au particles, randomly distributed over the surface of the silica core, range from 9 to 15 nm in size. The elemental mapping images of a  $\text{SiO}_2$ -Au-Pt nanoparticle synthesized with a higher amount of Pt precursor (39  $\mu\text{L}$  of  $\text{H}_2\text{PtCl}_6$ ) are presented in Fig. 1d-h. It can be seen that Pt preferentially deposits onto the Au surface, forming a thin layer of Pt covering the surface of each decorating Au particle. EDS measurements of the  $\text{SiO}_2$ -Au-Pt heterostructure revealed an elemental composition of Pt and Au of 2.34% and 11.20%, respectively.

The optical extinction spectra of the nanoparticles dispersed in water and measured after each fabrication step are shown in Fig. 2a. The extinction of the  $\text{SiO}_2$  nanoparticle solution monotonically decreases with wavelength, as expected. After the deposition of Au seeds, a plasmonic resonant peak starts to appear in the visible wavelength range. The extinction spectrum of the synthesized  $\text{SiO}_2$ -Au nanoparticles exhibits a broad localized surface plasmon resonance, typically between 500–700 nm, with the peak maximum around 560 nm, as shown in

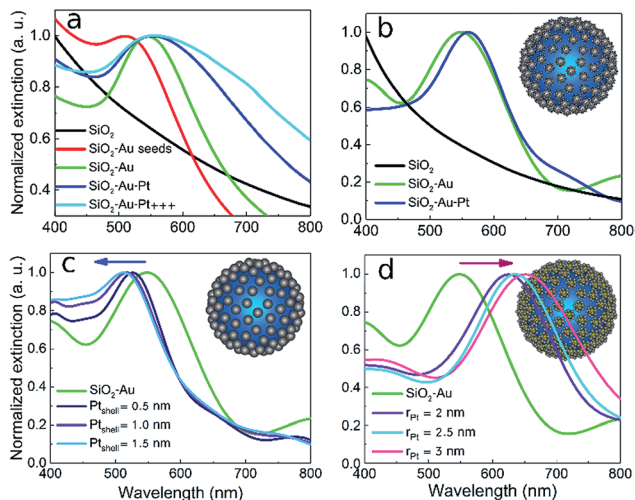


Fig. 2 (a) Experimental extinction spectra of the heterostructures at various synthesis stages. (b) Calculated extinction spectra of the heterostructures for a  $\text{SiO}_2$  particle diameter of 150 nm, Au particle diameter  $d = 15$  nm and elevation distance of the center of the Au nanoparticle from the silica surface  $3d/8$ , Pt shell thickness of 0.5 nm and Pt particle diameter of 2 nm. (c and d) Calculated extinction spectra for the limiting cases of Pt deposition on Au nanoparticles: Pt shells of various thicknesses (c) and Pt hemispheres of various radii (d); all the other parameters are as in (b). Insets (b–d): schematics of the modelled heterostructures used for the numerical simulations.

Fig. 2a (green curve). The resonance red shifts as the Au nanoparticle size increases which is in agreement with previous observations.<sup>18</sup> A further  $\sim 10$  nm red shift of the resonance is observed after deposition of Pt, together with a broadening of the peak. This effect has been reported previously in unsupported Au nanoparticles covered with Pt.<sup>21</sup> At higher Pt loading the extinction further broadens and red shifts (Fig. 2a).

To gain insight into the experimental findings numerical simulations of the scattering of light on the studied nanostructure at different fabrication stages were performed (Fig. 2b–d). As the average distance between the individual  $\text{SiO}_2$  nanoparticles estimated from the concentration of the solution used in the experiments was found to be  $\sim 2 \mu\text{m}$ , the particles were considered to be optically isolated and, therefore, the scattering on an individual nanostructure was numerically studied. The geometrical parameters of the nanostructure were derived from the sample TEM images and material analysis (Fig. 1). The structures were modelled considering a uniform distribution of 130 Au nanoparticles with a 15 nm diameter attached onto the surface of a  $\text{SiO}_2$  particle having a diameter of 150 nm. The extinction cross-sections derived from the simulations are in very good agreement with the experimental observations. For simplicity, the shape of the Au particles deposited on the  $\text{SiO}_2$  sphere were considered to be spherical, truncated by the  $\text{SiO}_2$  particle boundary.

A significant dependence of the resonance wavelength of the system on the distance between the centre of the Au sphere and  $\text{SiO}_2$  particle surface was observed, which is the result of the change in the position of plasmonic resonance

of the Au nanoparticles with their shape. The optimal separation distance resulting in the correct position of the plasmonic peak of the overall nanostructure was found to be  $3d/8$ , where  $d$  is the Au sphere diameter (Fig. 2b, green curve). As derived from the elemental mapping, Pt was present only on the surface of the Au nanoparticles. To model the resulting Pt distribution several approaches were implemented: (1) a uniform Pt shell on Au nanoparticles with a thickness from 0.5 to 1.5 nm, (2) Pt hemispheres with a diameter from 2 to 3 nm on the surface of the Au nanoparticles and (3) a combination of the Pt shell and hemispheres with the same dimensions as described above. In the limit of a uniform Pt shell deposition, a strong blue shift of the resonance is observed with increasing shell thickness (Fig. 2c). With increasing Pt content, the plasmonic resonance peak moves towards the one of a purely Pt particle, in the UV spectral range. This trend is in agreement with previous calculations by Zhang *et al.*<sup>28</sup> On the other side, in the limit of Pt hemispheres formed on the surface of Au nanoparticles, the plasmonic resonance of the overall nanostructure is red shifted, as can be seen in Fig. 2d. This suggests a strong influence on the optical properties by the shape effects. Combining these two cases together, a very good agreement with the position of the experimentally observed extinction peak was obtained, suggesting that, in addition to the thin layer of Pt formed after deposition, small Pt clusters are formed on the surface of the Au particles. The resultant extinction spectrum of the model is presented in Fig. 2b (blue curve), while the derived nanostructure geometry replicating the experimental results is presented in the inset.

### 3.2 Photocatalytic activity

Photocatalytic experiments were first carried out under visible-light illumination (450–1200 nm) for a period of 4 hours, with an average power of 40 mW. First, a control experiment was performed to determine the extent of degradation of methylene blue by photolysis only. Under the same experimental conditions, photodegradation was studied in the presence of the plasmonic heterostructures SiO<sub>2</sub>-Au and SiO<sub>2</sub>-Au-Pt, in order to compare the effects of the different catalysts on the degradation of methylene blue. Fig. 3a–c show the time evolution of the absorbance spectra of methylene blue. It can be seen that both in absence of nanoparticles (photolysis) and with the presence of SiO<sub>2</sub>-Au the photodegradation was similar over the time period of irradiation, indicating that the catalytic activity of the plasmonic heterostructure, under these conditions, is negligible due to fast electron–hole recombination. In contrast, the degradation rate in the presence of Pt on the catalyst is increased. These results are summarized in Fig. 3d, where the degradation percentages of the processes are presented. Pt plays an important role in determining the catalyst efficiency by providing active catalytic sites, where photogenerated hot carriers interact with adsorbates, and by preventing plasmonically-derived electron–hole recombination in Au, therefore improving catalytic performance of plasmonic nanostructures.

The effect of the Pt concentration in the SiO<sub>2</sub>-Au-Pt heterostructures was investigated under 556–566 nm illumination, which overlaps with the localized plasmon resonance of the nanoparticles of four different catalysts: samples Pt, Pt+, Pt++ and Pt+++ . As a control experiment, a methylene blue mixture without catalysts was used and resulted in a 3.7% degradation by photolysis only. An

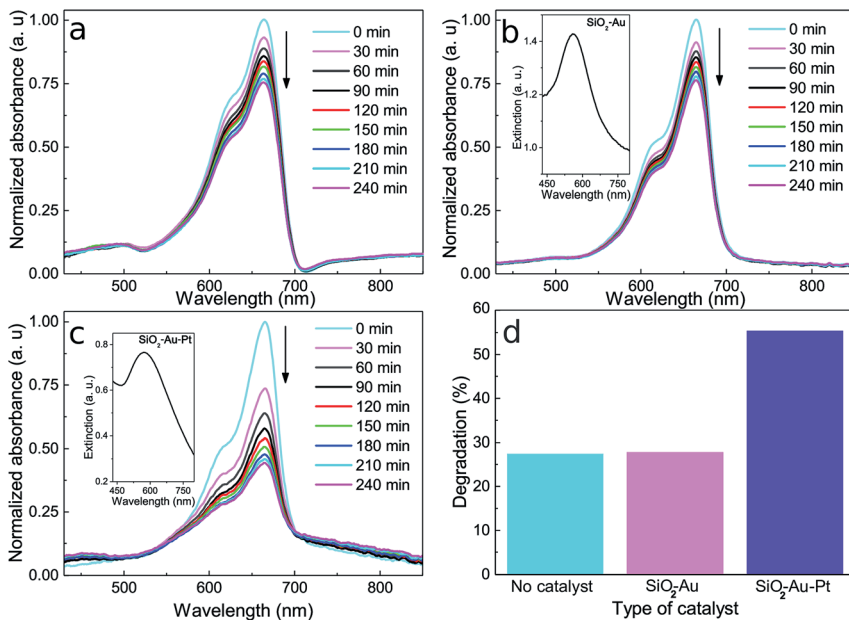


Fig. 3 Time evolution of absorption spectra of methylene blue during photodegradation, under white light irradiation: (a) photolysis, (b)  $\text{SiO}_2\text{-Au}$  and (c)  $\text{SiO}_2\text{-Au-Pt}$  heterostructures. (d) Degradation percentage of methylene blue, after 4 hours, for different types of heterostructures. Insets: extinction spectra of the heterostructures dispersed in water used in (b) and in (c).

increase of the degradation reaction rate was observed with the increase in Pt loading on the nanoparticles (Fig. 4). This results from an increased number of hot carriers extracted through the small Pt clusters, efficiently generated in the Au nanoparticles under resonant excitation. The highest efficiency was reached in the case of the  $\text{SiO}_2\text{-Au-Pt+++}$  heterostructures, with a 23-fold increase in the percentage of degraded methylene blue compared to the control experiment (Fig. 4). Even though the addition of Pt on the heterostructure is beneficial for the

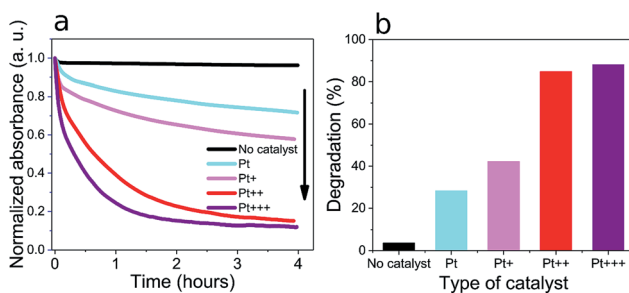


Fig. 4 (a) Time evolution of normalized absorbance and (b) absolute percentage of methylene blue degradation by the  $\text{SiO}_2\text{-Au-Pt}$  heterostructures with different Pt loadings, under 556–566 nm illumination (the amount of Pt loading increases from Pt to Pt+++).

catalytic activity, a limit of performance is expected, as a thicker layer of Pt would hinder hot carriers from reaching the surface and prevent any chemical reaction from taking place with an external adsorbate.

During this kind of photocatalytic process, highly reactive species that chemically interact with organic molecules are produced, such as superoxide anion radicals ( $\cdot\text{O}_2^-$ ) and hydroxyl radicals ( $\cdot\text{OH}$ ), due to the interaction of hot carriers with the surrounding aqueous medium. In general, the steps involved in the mechanism of photodegradation of methylene blue molecules in aqueous heterogeneous suspensions are related to hot carriers created after photon absorption by the catalyst, which are able to reach the surface and interact with externally placed molecules.<sup>21,29</sup> Once on the surface, excited electrons can ionize oxygen diatomic molecules ( $\text{O}_2$ ) on the catalyst surface, producing superoxide anion radicals. Also, excited holes can neutralize hydroxide ions ( $\text{OH}^-$ ) from water and produce hydroxyl radicals. The efficiency of these processes depends on the lifetime of the hot carriers, which can be controlled *via* the Pt loading of the Au nanoparticles. Lastly, the degradation of methylene blue can occur by chemical interaction with the generated superoxide and hydroxyl radicals.

## 4 Conclusions

Plasmonic  $\text{SiO}_2$ -Au-Pt hetero-nanoparticles were synthesized and their hot-electron extraction capabilities for catalytic performance assessed. It was found that the presence of Pt enhances hot-electron extraction efficiency, as compared to bare  $\text{SiO}_2$ -Au nanoparticles. Even though plasmonic semiconductor-noble metal hybrid nanostructures are under constant study,  $\text{SiO}_2$ -core based nanoparticles were chosen instead due to the dielectric properties of  $\text{SiO}_2$ , so that a Schottky barrier between metal and semiconductor is avoided, and thus more hot-carriers are available for reduction processes. The Pt loading has been shown to affect the hot-electron extraction rate, with higher quantities of Pt allowing increased catalytic activity, due to the increased carrier lifetime until highest performance was reached. This saturation of performance is expected, as a thicker layer of Pt on the Au hinders hot-carriers from reaching the surface, thus lowering their interaction rate with an external adsorbate. The comparison between TEM measurements and numerical modelling of the extinction spectra indicates that small Pt clusters are formed in addition to the Pt shells on the Au nanoparticles. This might increase the availability of charge carriers for catalysis at the active sites on the surface of Pt, improving the catalytic activity by facilitating hot-carrier extraction through the interface. Plasmonic hybrid bimetallic nanoparticles show interesting attributes for hot carrier technologies, and heterostructures significantly increase the catalytic activity of hot carriers by controlling their lifetime. The properly designed plasmonic heterostructures allow optimization and exploitation of the full potential of plasmonically derived hot-carriers.

## Conflicts of interest

There are no conflicts to declare.

## Acknowledgements

This work was supported by EPSRC (UK) under the Reactive Plasmonics Programme grant. J. U. S. G acknowledges a studentship from CONACYT-Mexico. M. R. G acknowledges a studentship from SENER-CONACYT-Mexico. M. R. G. is grateful to M. F. Picardi for helpful discussions of the numerical simulations. All the data supporting this research are provided in full in the results section.

## References

- 1 S. Linic, P. Christopher and D. B. Ingram, *Nat. Mater.*, 2011, **10**, 911–921.
- 2 W. Hou and S. B. Cronin, *Adv. Funct. Mater.*, 2012, **23**, 1612–1619.
- 3 Z. Liu, W. Hou, P. Pavaskar, M. Aykol and S. B. Cronin, *Nano Lett.*, 2011, **11**, 1111–1116.
- 4 P. Wang, A. V. Krasavin, M. E. Nasir, W. Dickson and A. V. Zayats, *Nat. Nanotechnol.*, 2018, **13**, 159–164.
- 5 J. Lee, S. Mubeen, X. Ji, G. D. Stucky and M. Moskovits, *Nano Lett.*, 2012, **12**, 5014–5019.
- 6 S. Mubeen, J. Lee, N. Singh and M. Moskovits, *Nat. Nanotechnol.*, 2013, **8**, 247–251.
- 7 S. Mubeen, J. Lee, D. Liu, G. D. Stucky and M. Moskovits, *Nano Lett.*, 2015, **15**, 2132–2136.
- 8 B. Wu, D. Liu, S. Mubeen, T. T. Chuong, M. Moskovits and G. D. Stucky, *J. Am. Chem. Soc.*, 2016, **138**, 1114–1117.
- 9 Z. Zheng, T. Tachikawa and T. Majima, *J. Am. Chem. Soc.*, 2014, **136**, 6870–6873.
- 10 Z. Lou, M. Fujitsuka and T. Majima, *ACS Nano*, 2016, **10**, 6299–6305.
- 11 H. Robatjazi, S. M. Bahauddin, C. Doiron and I. Thomann, *Nano Lett.*, 2015, **15**, 6155–6161.
- 12 S. Mukherjee, F. Libisch, N. Large, O. Neumann, L. V. Brown, J. Cheng, J. B. Lassiter, E. A. Carter, P. Nordlander and N. J. Halas, *Nano Lett.*, 2012, **13**, 240.
- 13 S. Mukherjee, L. Zhou, A. M. Goodman, N. Large, C. Ayala-Orozco, Y. Zhang, P. Nordlander and N. J. Halas, *J. Am. Chem. Soc.*, 2014, **136**, 64–67.
- 14 L. Zhou, C. Zhang, M. J. McClain, A. Manjavacas, C. M. Krauter, S. Tian, F. Berg, H. O. Everitt, E. A. Carter, P. Nordlander and N. J. Halas, *Nano Lett.*, 2016, **16**, 1478–1484.
- 15 M. Pirhashemi and A. Habibi-Yangjeh, *J. Colloid Interface Sci.*, 2017, **491**, 216–229.
- 16 S. Dong, J. Feng, M. Fan, Y. Pi, L. Hu, X. Han, M. Liu, J. Sun and J. Sun, *RSC Adv.*, 2015, **5**, 14610–14630.
- 17 R. A. Rather, S. Singh and B. Pal, *J. Nanosci. Nanotechnol.*, 2017, **17**, 1210–1216.
- 18 B. E. Brinson, J. B. Lassiter, C. S. Levin, R. Bardhan, N. Mirin and N. J. Halas, *Langmuir*, 2008, **24**, 14166–14171.
- 19 M. J. García-Soto and O. González-Ortega, *Gold Bull.*, 2016, **49**, 111–131.
- 20 R. Bardhan, S. Lal, A. Joshi and N. J. Halas, *Acc. Chem. Res.*, 2011, **44**, 936–946.
- 21 D. Kumar, S. B. Lee, C. H. Park and C. S. Kim, *ACS Appl. Mater. Interfaces*, 2018, **10**, 389–399.
- 22 D. G. Duff, A. Baiker and P. P. Edwards, *Langmuir*, 1993, **9**, 2301–2309.
- 23 W. Stöber, A. Fink and E. Bohn, *J. Colloid Interface Sci.*, 1968, **26**, 62–69.

- 24 P. Wang, A. V. Krasavin, F. N. Viscomi, A. M. Adawi, J.-S. G. Bouillard, L. Zhang, D. J. Roth, L. M. Tong and A. V. Zayats, *Laser Photonics Rev.*, 2018, **12**, 201800179.
- 25 P. B. Johnson and R. W. Christy, *Phys. Rev. B*, 1972, **6**, 4370–4379.
- 26 W. S. M. Werner, K. Glantschnig and C. Ambroxsch-Draxl, *J. Phys. Chem. Ref. Data*, 2009, **38**, 1013–1092.
- 27 C. M. Copley, J. Chen, E. C. Cho, L. V. Wang and Y. Xia, *Chem. Soc. Rev.*, 2011, **40**, 44–56.
- 28 C. Zhang, B. Q. Chen and Z. Y. Li, *J. Phys. Chem.*, 2015, **119**, 16836–16845.
- 29 A. Houas, H. Lachheb, M. Ksibi, E. Elaloui, C. Guillard and J. M. Herrmann, *Appl. Catal., B*, 2001, **31**, 145–157.